JOURNAL OF GEOPHYSICAL RESEARCH, VOL. 90, NO. B1, PAGES 605–621, JANUARY 10, 1985

Geometric Effects of Global Lateral Heterogeneity on Long-Period Surface Wave Propagation

THORNE LAY

Department of Geological Sciences, University of Michigan, Ann Arbor

HIROO KANAMORI

Seismological Laboratory, California Institute of Technology, Pasadena

Long-period Rayleigh waves from Iranian earthquakes have large amplitude asymmetries between minor arc and major arc arrivals (e.g., R_2 and R_3) at digital stations in the azimuth range N20°W to N60°E. These asymmetries are as large as a factor of 2 at a period of 256 s and persist to periods greater than 300 s. In some cases the entire Rayleigh wave group arrival spanning periods from 100 to 300 s is either uniformly enhanced in amplitude or diminished to such a degree that the group arrival appears to be missing. The amplitude anomalies are generally not accompanied by significant phase anomalies. The irregular azimuthal distribution of the amplitude asymmetries and their occurrence for events with different focal mechanisms and epicentral separations of several hundred kilometers preclude an explanation of these observations by source complexity. Events in the Mediterranean and Nepal do not produce similar amplitude asymmetries at the same stations. The anomalies are thus most likely due to focusing and defocusing propagation effects. As a preliminary investigation of the effects of lateral heterogeneity of upper mantle velocity structure on long-period surface wave amplitudes, surface wave ray-tracing calculations are performed using recently proposed global phase velocity distributions. Dramatic deviations from great circle paths are predicted for long propagation paths (e.g., R_3). The particular spatial distribution of lateral velocity gradients around a given source location determines whether substantial amplitude asymmetries will be observed between minor arc and major arc arrivals and whether these will persist for sequential great circle orbits. The 200-s period amplitude asymmetry observed at KIP for the Iranian source region ($R_{2,4} \gg R_3$) is well predicted by the ray-tracing results. The absence of this anomaly for the other source regions is also predicted. Other observed anomalies are not all well predicted, but it is clear that geometric effects can contribute significantly to the observed variations of Rayleigh and Love wave amplitudes. This is the probable explanation for the instability of Q estimates made from surface waves. Other source regions producing large surface wave amplitude anomalies include Japan and southeastern Alaska.

INTRODUCTION

With the advent of high-quality digital seismic networks, long-period (>100 s) surface waves have been utilized extensively in inversion for earthquake source mechanisms [*Kanamori and Given*, 1981, 1982; *Dziewonski and Woodhouse*, 1983; *Dziewonski et al.*, 1983] and inversion for lateral heterogeneity of the upper mantle [*Nakanishi and Anderson*, 1982, 1983, 1984; *Woodhouse*, 1983; *Woodhouse and Dziewonski*, 1984; *Masters et al.*, 1982]. The apparent success of these techniques testifies to the general stability of long-period surface wave propagation, particularly for the phase of spheroidal modes. Rayleigh waves with periods from 200 to 300 s generally show predictable amplitude behavior as well [*Kanamori and Given*, 1981]. However, the amplitude and phase scatter is significantly larger for shorter-period Rayleigh waves and for Love waves of all periods, which is usually attributed to the greater sensitivity of these phases to lateral variations in the upper 200 km of the mantle. There are also several events for which large long-period Rayleigh wave amplitude anomalies have been observed [*Niazi and Kanamori*, 1981; *Buland and Taggart*, 1981], which are not easily explained by source processes. The purpose of this paper is to document examples of anomalous long-period surface wave amplitude behavior and to provide a preliminary appraisal of the effects of global lateral heterogeneity on surface wave propagation from a ray theory perspective.

Paper number 4B5035.
0148-0227/85/004B-5035$05.00

OBSERVATIONS

The 1978 Tabas, Iran, earthquake (Table 1) produced some of the most remarkable long-period surface wave anomalies described in the literature. In an analysis of International Deployment of Accelerometers (IDA) recordings for this event, *Niazi and Kanamori* [1981] observed large-amplitude asymmetries between minor arc and major arc Rayleigh wave arrivals at stations in the azimuth range N10°W to N40°E. The records from these stations are shown in Figure 1. Entire group arrivals show clear amplitude asymmetries at all three stations, with Rayleigh waves that have traveled farther having larger amplitudes than shorter path arrivals that left the source in the opposite direction (e.g., $|R_4| > |R_3|$ at PFO and KIP, and $|R_5| > |R_4|$ at CMO). CMO shows an opposite pattern of asymmetry to that at PFO and KIP despite being tightly bracketed in azimuth by the other two stations. The R_3 arrival at PFO and the R_4 arrival at CMO have very little energy, and the Rayleigh wave group arrivals are essentially missing. This is particularly striking since all three stations lie in a stable portion of the radiation pattern for this thrust event [*Niazi and Kanamori*, 1981]. Given the seismic moment of this event of 1.4×10^{20} N m and an estimated source dimension of 80 km, it is not possible to account for the observed asymmetries by source finiteness. Figure 2 emphasizes this, for it shows that when Gaussian band-pass filters with successively longer-period high-pass cutoffs are applied to the KIP record, the amplitude asymmetries persist to very long periods. Noting that the dominant periods of the filtered traces are about 50 s longer than the short-period cutoff, it is clear that even 250-s period energy shows substantial asym-

TABLE 1. National Earthquake Information Service Epicentral Parameters of the Earthquakes Analyzed in This Study

Location	Date	Origin Time	Latitude	Longitude	M_s
Tabas, Iran	Sept. 16, 1978	1535:56.6	33.386°N	57.434°E	7.4
Quainat, Iran	Nov. 14, 1979	0221:22.1	33.918°N	59.741°E	6.6
Quainat, Iran	Nov. 27, 1979	1710:32.9	34.134°N	59.877°E	7.1
Sirch, Iran	June 11, 1981	0724:25.2	29.913°N	57.715°E	6.7
Sirch, Iran	July 28, 1981	1722:24.6	30.013°N	57.794°E	7.1
Yugoslavia	April 15, 1979	0619:44.1	42.096°N	19.209°E	6.9
Aegean	Dec. 19, 1981	1410:50.7	39.243°N	25.227°E	7.2
Italy	Nov. 23, 1980	1834:53.3	40.914°N	15.366°E	6.9
Nepal	July 29, 1980	1458:40.8	29.598°N	81.092°E	6.5
Akita-Oki, Japan	May 26, 1983	0259:59.6	40.462°N	139.102°E	7.7
St. Elias, Alaska	Feb. 28, 1979	2127:06.1	60.642°N	141.593°W	7.1

metry. After equalizing the propagation distances, the 256-s spectral amplitudes of the even order number arrivals (R_2, R_4, R_6) are all a factor of 2 greater than those of the odd order number arrivals (R_3, R_5). The asymmetries persist to a period of 300 s for CMO and PFO as well. *Niazi and Kanamori* [1981] did not provide an explanation for these observations but speculated that regional structural heterogeneities near the source or along the propagation paths, or possibly fault plane complexity, could explain the asymmetry. We will investigate these possibilities further.

The presence of strong amplitude anomalies is a potential source of bias in source mechanism determination using long-period surface waves, yet it is necessary to know the mechanism in order to appraise the anomalies. To minimize this problem, we supplement the IDA observations for the Tabas earthquake with Rayleigh and Love wave observations from the Global Digital Seismographic Network (GDSN). Figure 3 shows the distribution of stations about the Iranian source region. Unfortunately, no additional GDSN stations lie in the azimuth range spanned by PFO and KIP, though stations ANMO and MAJO lie just outside this range. Adopting the procedures described by *Kanamori and Given* [1981] and *Lay et al.* [1982], the IDA and GDSN Rayleigh and Love wave data are combined in a moment tensor inversion. Following *Niazi and Kanamori* [1981], we adopt a source process time τ of 33 s, and a source depth of 16 km. To remove the ill conditioning of the inversion for this shallow depth, we constrain $M_{zx} = M_{zy} = 0$ [*Kanamori and Given*, 1981], and the resulting moment tensor and double-couple decomposition are listed in Table 2. The results are very similar to those found using IDA data alone [*Niazi and Kanamori*, 1981, Table 2] with well-resolved moment tensor elements and a very small minor double couple. Since first-motion data [*Berberian et al.*, 1979] constrain one of the nodal planes very well, we fix this plane and perform a fault model inversion to determine the slip angle λ and the scalar moment M_0. The results are given in Table 2, and these again agree closely with the previous modeling.

The 256-s period spectra for the Tabas earthquake are plotted in Figure 4, along with the theoretical spectra for the fault model inversion in Table 2. The observed Rayleigh wave phase shows a systematic, but minor, azimuthal variation, which appears to be unrelated to the large-amplitude asymmetries. ANMO has an amplitude asymmetry very similar to that of the adjacent IDA station PFO, while MAJO shows a weak pattern similar to that of CMO. The interfingering of the amplitude asymmetries is suggestive of a focusing/defocusing amplitude interference pattern. Because the source mechanism inversions apply least squares criteria, we cannot easily identify whether the minor arc or the major arc arrivals, or both have anomalous amplitudes, though it seems likely that the R_2 signal at KIP is anomalously large. Table 3 lists ratios of the observed 256-s period spectral amplitudes for IDA stations divided by the calculated values for the fault model in Table 2. The absolute level of the ratio for a given arrival is sensitive to the accuracy of the source model and reference earth Q model, particularly for nodal stations; however, any asymmetry between arrivals at a given station is not accounted for by the source model.

The only Love wave observations in the azimuth range of

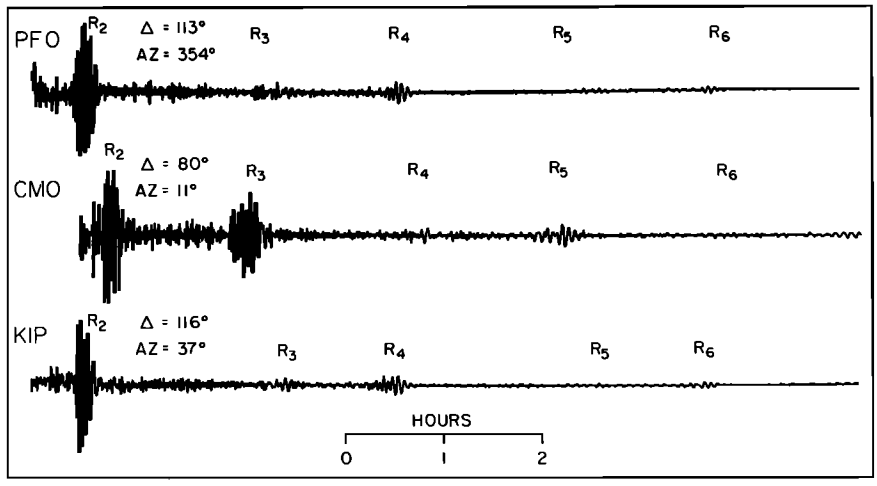

Fig. 1. IDA recordings of Rayleigh wave arrivals for the September 16, 1978, Tabas, Iran, earthquake.

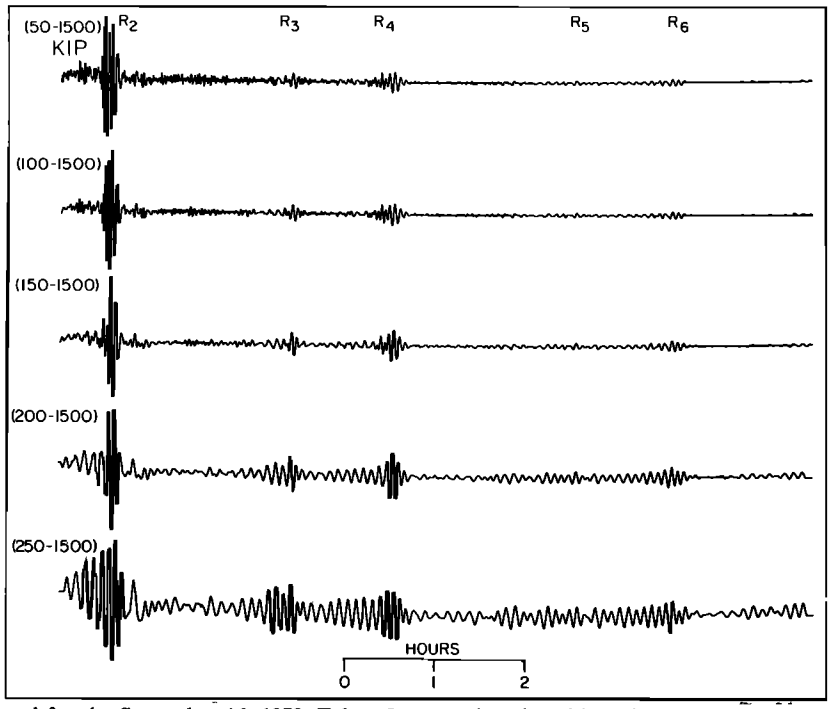

Fig. 2. KIP record for the September 16, 1978, Tabas, Iran, earthquake with various Gaussian band-pass filters. The short- and long-period cutoffs of the filters are shown at the left of each trace.

the anomalous Rayleigh wave behavior are from MAJO, which shows little asymmetry, and from ANMO, which shows an asymmetry similar to that for the Rayleigh waves at the same station. The latter factor of 2 asymmetry appears to be larger than the typical scatter of $\simeq 30\%$ for nonnodal Love wave amplitudes at other azimuths. The ANMO G_2 arrival also has the largest phase anomaly. Ultra-long-period recordings at Pasadena show similar patterns of Rayleigh and Love wave amplitude asymmetry to those at PFO and ANMO.

The most straightforward approach to interpreting the amplitude asymmetries is to determine whether they are observed for other events. Figure 5 compares recordings at KIP for several other Iranian earthquakes as well as for two events in the Mediterranean. The latter two events show a normal variation of amplitude between R_2, R_3, and R_4, whereas the Iranian events produced signals very similar to that for the Tabas earthquake shown in Figure 1. Table 1 gives the locations of the Iranian earthquakes, which are separated by several

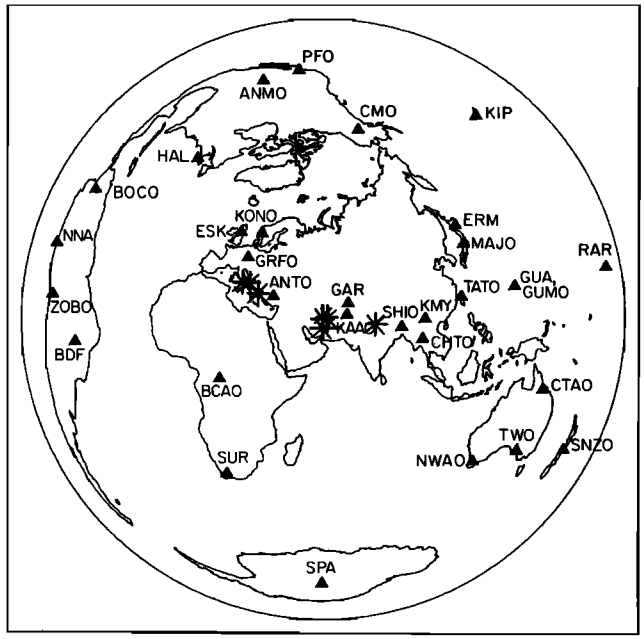

Fig. 3. Equidistance azimuthal plot centered on the Iranian source region showing the location of IDA and GDSN stations. The epicenters of the events in Table 1 are indicated by the asterisks.

TABLE 2. Source Parameters of the September 16, 1978, Tabas, Iran, Earthquake From Combined Rayleigh and Love Wave Moment Tensor Inversion (Model 1) and Fault Model Inversion (Model 2) at the Period 256 s

Source Parameter	Value
Model 1	
M_{xy}*	0.58 ± 0.05
$M_{yy} - M_{xx}$	-0.13 ± 0.11
$M_{yy} + M_{xx}$	-1.16 ± 0.08
Model 2	
M_0	1.37 ± 0.08
ϕ (constrained)	127°
δ (constrained)	62°
λ	$79° \pm 2.5°$
rms	0.636
Major Double Couple	
M_0	1.17
ϕ	138°
δ	45°
λ	90°
Minor Double Couple 0.8%	
rms	0.659

$\tau = 33$ s; $d = 16$ km.

*The units of the moment tensor M_{ij} and the scalar moment M_0 are 10^{20} N m.

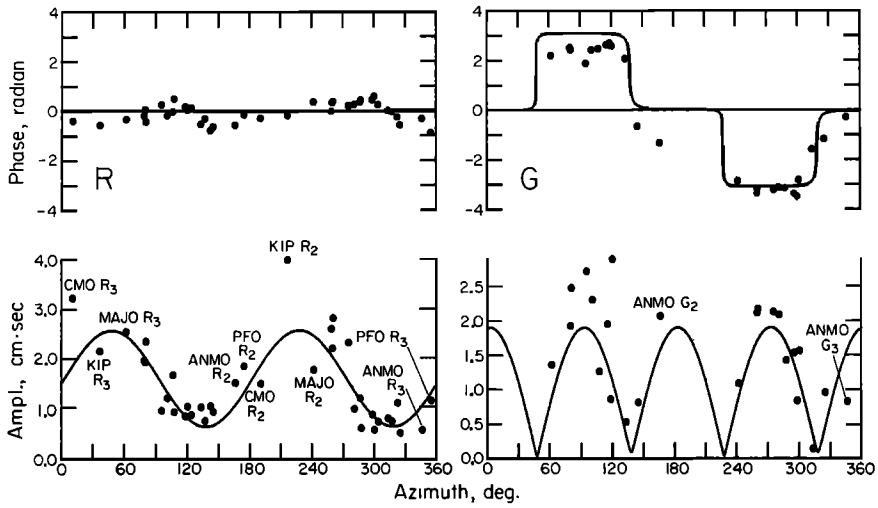

Fig. 4. Rayleigh wave and Love wave spectra for the 256-s period arrivals for the Tabas earthquake. The curves indicate the spectra for the major double couple of the fault model in Table 2. Stations with strong amplitude asymmetries are labeled.

hundred kilometers. This indicates that very localized source region velocity structure is not responsible for the anomalies at KIP.

In order to constrain further the surface wave anomaly behavior, we perform moment tensor and fault model inversions for four additional Iranian earthquakes, two earthquakes in the Mediterranean, and an earthquake in Nepal. The epicentral parameters are listed in Table 1, and the locations are shown in Figure 3. The Iranian observations are summarized in Figure 6, where 256-s spectra are compared with inversion models. Figure 6*a* shows Rayleigh and Love wave spectra for the November 27, 1979, event (Table 1), which occurred in the same region as the November 14, 1979, earthquake. The moment tensor solution given in Table 4 has a small minor double couple, and the event involved predominantly vertical left-lateral strike-slip faulting trending nearly east-west. This fault plane is selected on the basis of the 60-km-long ground breakage [*Haghipour and Amidi*, 1980]. The amplitude spectra show very similar variations to those for the November 14 event, which was also a strike-slip event, with a factor of 2 asymmetry at KIP and subdued asymmetries at CMO, SUR, and PFO. The ANMO Love wave asymmetry is like that found for the 1978 Tabas event (Figure 4). Figure 6*b* shows the Rayleigh and Love wave spectra for the June 11, 1981, Sirch, Iran, earthquake in southeastern Iran. The moment tensor inversion has a large minor double couple, suggesting a strong oblique component. Using first-motion data, we constrain the strike and dip of one fault plane and invert for the fault model in Table 4. This solution is indicated by dashed lines in Figure 6*b* and fits the data as well as the moment tensor solution. There are strong Rayleigh wave amplitude asymmetries at KIP and ERM as well as at SPA, PFO, and ANMO. The phase behaves much more stably. The Love waves show increasing amplitude and phase asymmetry at ANMO for successive order number arrivals. The July 28, 1981, Sirch, Iran, event has similar strong amplitude asymmetries, but the source process appears to be complex [*Dziewonski and Woodhouse*, 1983], which complicates interpreting the anomalies.

The Iranian events show consistent patterns of asymmetry for the entire range of thrust, oblique, and strike-slip faulting events in the three source regions investigated. This is clear

TABLE 3. Observed Rayleigh Wave Amplitude Anomalies for 1978 Tabas, Iran, Earthquake

	R_2	R_3	R_4	R_5	R_3/R_2
CMO	0.80	1.73	0.57	2.11	2.16
ESK*	1.19	1.17	0.99	1.47	0.98
HAL*	1.62	1.71	1.26	2.10	1.06
KIP	1.59	0.86	1.66	0.79	0.54
NNA	1.43	1.03	1.93	1.02	0.72
PFO	1.39	0.88	1.54	0.82	0.63
RAR	1.26	0.95	1.34	0.82	0.75
TWO*	0.98	1.17	···	···	1.19

$T = 256$ s.
*Nodal stations.

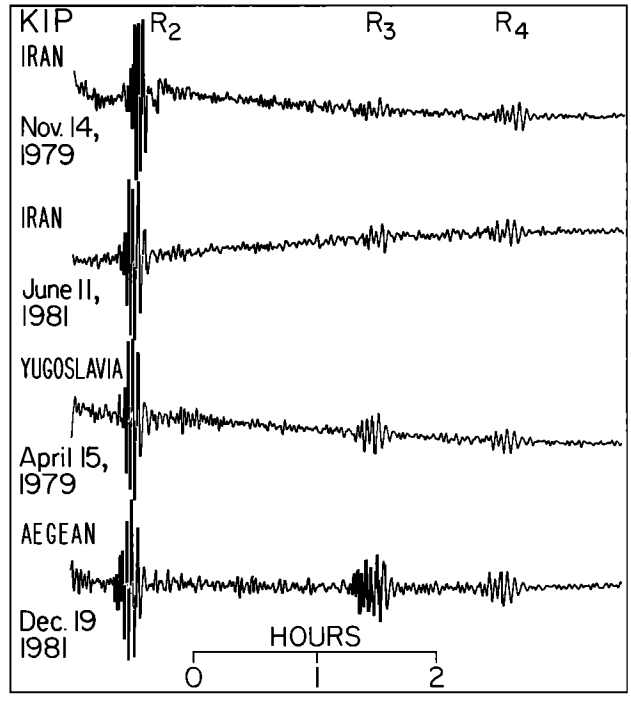

Fig. 5. Examples of Rayleigh wave arrivals recorded by KIP for events in Iran and the Mediterranean. Note the anomalous R_4/R_3 amplitude ratios for the Iranian events.

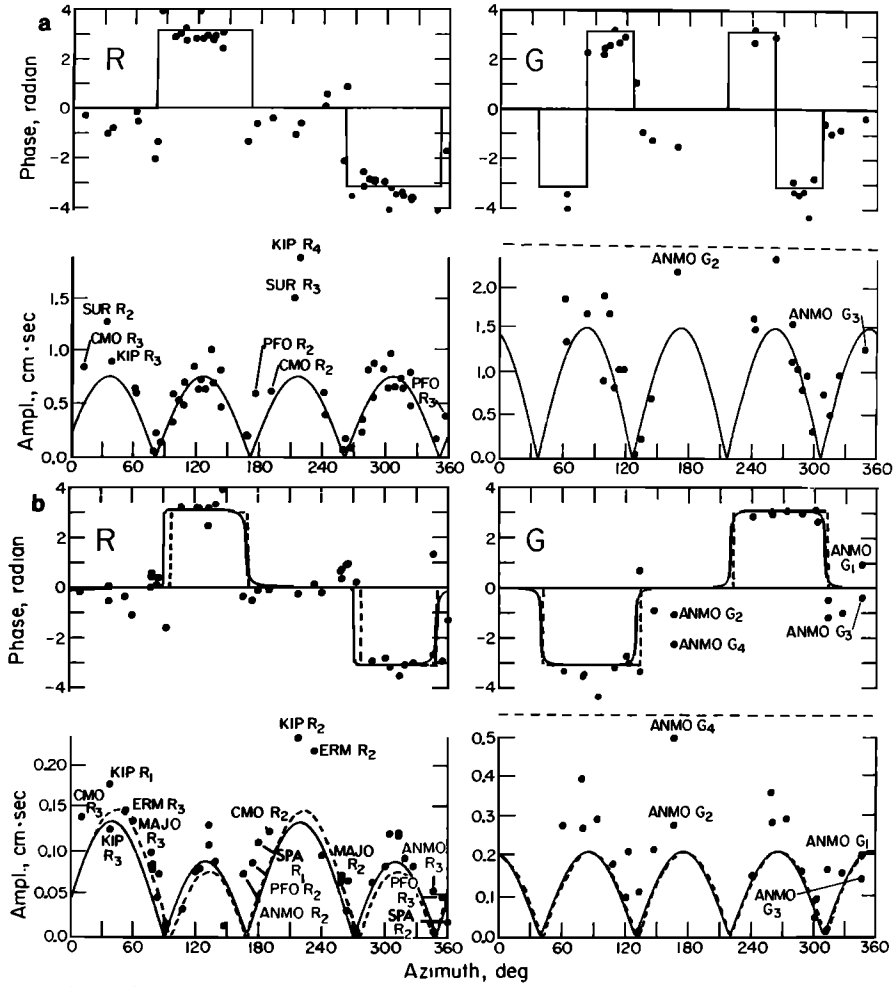

Fig. 6. (*a*) Rayleigh and Love wave spectra for a period of 256 s for the November 27, 1979, Iranian event. The curves are for the major double couple of the moment tensor solution in Table 4. (*b*) Rayleigh and Love wave spectra for a period of 256 s for the June 11, 1981, Iranian event. The solid curves are for the moment tensor solution in Table 4, and the dashed curves are for the fault model solution in the same table.

evidence for a propagational effect, which must be on a sufficiently large scale to affect the 256-s period energy. We attempt to constrain the location of this structure by investigating events to the east and to the west of Iran. *Kanamori and Given* [1981] show spectra for the April 15 Monte Negro, Yugoslavia, earthquake (Table 1), which has no evidence of asymmetry at KIP (see Figure 5) or other IDA stations. To corroborate this, we perform moment tensor inversions for the

TABLE 4. Constrained Moment Tensor and Fault Model Inversion Solutions for Iranian Earthquakes

Event	Nov. 14, 1979	Nov. 27, 1979	June 11, 1981	July 28, 1981
Data	IDA, *R* $\tau = 30$ s, $d = 16$ km	IDA, GDSN *R* and *G* $\tau = 30$ s, $d = 16$ km	IDA, GDSN *R* and *G* $\tau = 15$ s, $d = 16$ km	IDA, GDSN *R* and *G* $\tau = 20$ s, $d = 16$ km
M_{xy}*	0.084 ± 0.012	0.446 ± 0.034	0.068 ± 0.007	0.210 ± 0.032
$M_{yy} - M_{xx}$	0.128 ± 0.028	0.269 ± 0.069	0.014 ± 0.013	-0.047 ± 0.056
$M_{yy} + M_{xx}$	0.007 ± 0.010	-0.028 ± 0.049	-0.024 ± 0.009	-0.190 ± 0.039
Major double couple				
M_0	0.109	0.480	0.081	0.307
ϕ	161°	262°	267°	138°
δ	90°	90°	90°	45°
λ	180°	0°	0°	90°
Minor double couple	5.6%	5.8%	30.2%	38%
Fault model				
M_0			0.112 ± 0.036	
ϕ			268° (constrained)	
δ			85° (constrained)	
λ			$53° \pm 14°$	

$T = 256$ s.

*Units of moment tensor M_{ij} and scalar moment M_0 are 10^{20} N m.

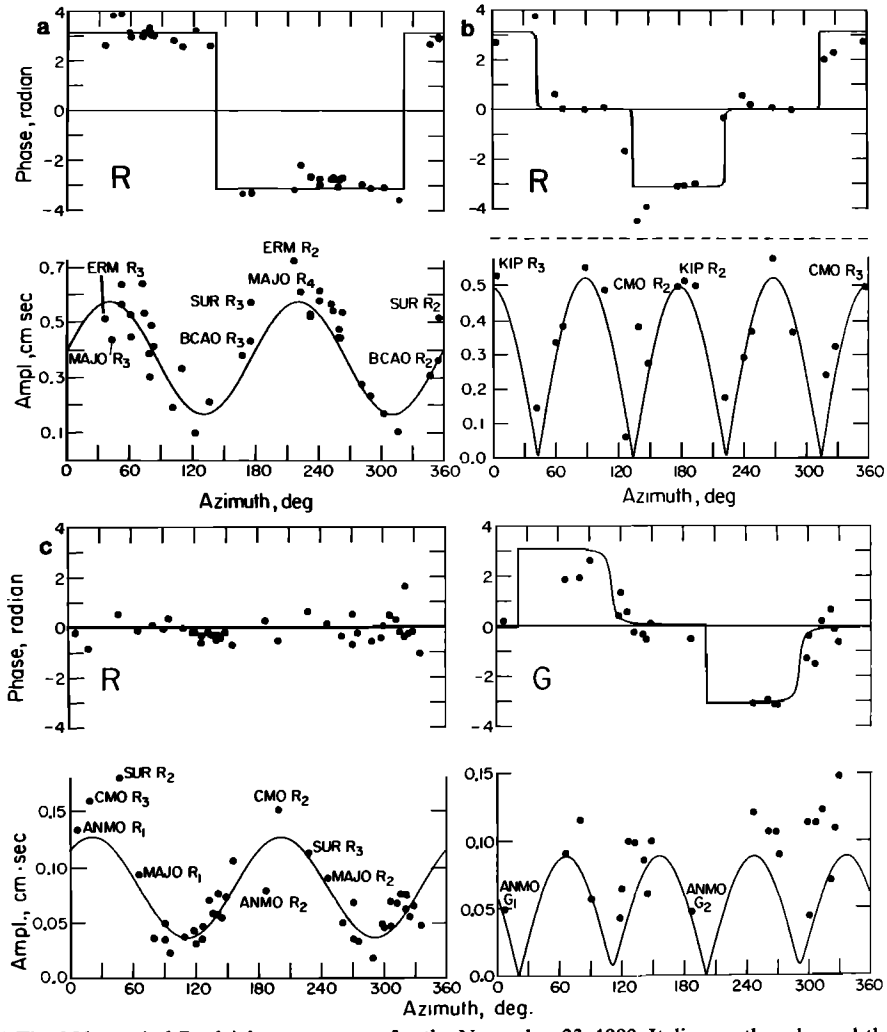

Fig. 7. (*a*) The 256-s period Rayleigh wave spectra for the November 23, 1980, Italian earthquake and the fault model in Table 5. (*b*) The 256-s period Rayleigh wave spectra for the December 19, 1981, Aegean earthquake and the fault model solution in Table 5. (*c*) The 256-s period Rayleigh and Love wave spectra for the July 29, 1980, Nepal earthquake and the fault model in Table 5.

November 23, 1980, Italian earthquake and the December 19, 1981, Aegean event (Table 1). The 256-s period Rayleigh wave spectra for these events are shown in Figures 7*a* and 7*b*, respectively. The data are compared with fault model solutions for which the strike and dip of one of the nodal planes is well constrained by first motions. The source parameters are included in Table 5, along with the results of constrained moment tensor inversions. Figure 7 shows that both the am-

TABLE 5. Constrained Moment Tensor and Fault Model Inversion Solutions for Non-Iranian Earthquakes

Event	Italy, Nov. 23, 1980	Aegean, Dec. 19, 1981	Nepal, July 29, 1980
Data	IDA, GDSN *R* and *G* τ = 20 s, *d* = 16 km	IDA *R* τ = 20 s, *d* = 16 km	IDA, GDSN *R* and *G* τ = 15 s, *d* = 16 km
M_{xy}*	−0.124 ± 0.014	0.017 ± 0.025	0.019 ± 0.003
$M_{yy} - M_{xx}$	−0.015 ± 0.280	−0.633 ± 0.050	0.045 ± 0.005
$M_{yy} + M_{xx}$	0.240 ± 0.019	−0.012 ± 0.019	−0.053 ± 0.004
Major double couple			
M_0	0.245	0.323	0.056
ϕ	313°	43°	110°
δ	45°	90°	45°
λ	270°	180°	90°
Minor double couple	0.1%	3.8%	4.9%
Fault model	τ = 45 s, *d* = 10 km	τ = 25 s, *d* = 16 km	τ = 15 s, *d* = 16 km
M_0	0.288 ± 0.015	0.325 ± 0.024	0.087 ± 0.006
ϕ	317° (constrained)	43° (constrained)	111° (constrained)
δ	63° (constrained)	76° (constrained)	70° (constrained)
λ	275.8° ± 2.6°	176.6° ± 6.4°	90.3° ± 4.0°

T = 256 s.
*Units of moment tensor M_{ij} and scalar moment M_0 are 10^{20} N m.

TABLE 6. Great Circle Phase Velocity and Attenuation Measurements

Event	Phase		Period, s 256.0	222.6	196.9	176.6	150.6
Sept. 16, 1978	KIP R_2R_4	C	4.952	4.715	4.547	4.429	4.297
		Q	184	181	158	153	138
	R_3R_5	C	4.944	4.684	4.531	4.420	4.290
		Q	159	127	128	111	170
	PFO R_2R_4	C	4.942	4.709	4.545	4.427	4.301
		Q	206	221	199	165	134
	CMO R_2R_4	C	4.949	4.735	4.559	4.453	4.298
		Q	109	120	106	92	98
	R_3R_5	C	4.951	4.712	4.548	4.429	4.297
		Q	232	181	159	133	111
Nov. 14, 1979	KIP R_2R_4	C	4.964	4.726	4.548	4.425	4.295
		Q	181	535	371	169	124
	PFO R_2R_4	C	4.930	4.173	4.548	4.424	4.297
		Q	253	325	189	178	157
	CMO R_1R_3	C	4.952	4.716	4.547	4.433	4.297
		Q	160	145	154	163	110
	R_2R_4	C	4.961	4.724	4.554	4.444	4.308
		Q	119	105	101	111	120
	SUR R_2R_4	C	4.951	4.710	4.561	4.434	4.255
		Q	163	147	120	114	114
	R_3R_5	C	4.955	4.712	4.570	4.424	...
		Q	164	129	95	106	...
Nov. 27, 1979	KIP R_3R_5	C	4.942	4.695	4.579	...	...
		Q	230	268	158	...	...
	PFO R_2R_4	C	4.939	4.708	4.542	4.425	4.298
		Q	217	276	239	224	192
	CMO R_2R_4	C	4.963	4.725	4.557	4.445	4.304
		Q	113	124	108	99	123
	R_3R_5	C	4.957	4.704	4.553	4.430	4.240
		Q	213	157	132	118	136

plitudes and phase are well matched for both events, with no significant asymmetry apparent at KIP, CMO, or SUR. There is a slight asymmetry for the Japanese stations ERM and MAJO for the Italian earthquake, with the even order number arrivals being somewhat enhanced. The Love wave observations for the Italian earthquake do not show strong asymmetries.

The closest earthquake located east of Iran with sufficient moment to generate adequate long-period surface waves on the digital network is the July 29, 1980, Nepal event. The Rayleigh and Love wave spectra for this event are shown in Figure 7*c*. The KIP record was not usable, but the other stations do not show amplitude variations like those seen for the Iranian events. CMO and MAJO do not have any asymmetry, while SUR and ANMO have asymmetries opposite in sense to those for the Iranian events. The Love waves show characteristic scatter but no asymmetry at ANMO. The theoretical curves are for a fault model inversion with the azimuth and dip constrained to satisfy first motion observations.

By referring to Figure 3, it is apparent that a relatively small variation in source location suffices to modify the amplitude asymmetry pattern significantly. The great circle paths from Iran to PFO, CMO, and KIP are only distinctive from the other source regions in that they pass along the eastern Africa rift valley or mid-Indian Ocean ridge systems. In order to test whether these great circles are particularly anomalous, we measure great circle phase velocity and attenuation [*Kanamori*, 1970] for several of the Iranian events. In this analysis we use only Rayleigh waves recorded by IDA instruments because of their superior long-period response compared to the GDSN instruments. Measurements for the stations with amplitude asymmetries are listed in Table 6. In calculating Q, the phase and amplitude spectra are smoothed over an effective frequency band of 0.8 mHz, corresponding to a period band of about 50 s for a 256-s period. The variation in great circle phase velocity has a small variance for each period, with total ranges less than 1%, and stations at other azimuths yield similar values. The variations for a given station are much smaller and do not differ significantly if odd or even order arrivals are used. This consistency reflects the lack of phase anomalies in the moment tensor inversions described above. The Q estimates appear to be much less stable, as has long been noted [*Kanamori*, 1970]. Some of the scatter results from the low signal-to-noise ratio for R_4 and R_5 arrivals from these events. Values are not given for periods where the amplitude spectra appear to be contaminated. There is a tendency for the relatively large-amplitude signals (e.g., R_2, R_4 at KIP; R_3, R_5 at CMO) to give higher Q estimates than for the complementary arrivals at the same station. This is suggestive of focusing or defocusing effects rather than intrinsic attenuation, but the scatter is so large that it is difficult to quantify these effects. This will be addressed further in the discussion.

SURFACE WAVE RAY TRACING

It is well known that lateral heterogeneity of velocity structure produces large-amplitude variations of short-period (20 s) surface waves due to multipathing and focusing effects [e.g., *McGarr*, 1969; *Capon*, 1970]. Several investigators have applied surface wave ray tracing to characterize these short-period effects and have shown that significant deviations from great circle paths are expected [*Gjevik*, 1974; *Sobel and von Seggern*, 1978]. We adopt a similar approach in analyzing longer-period Rayleigh wave effects caused by global lateral heterogeneity. While ray theory does not easily extend to con-

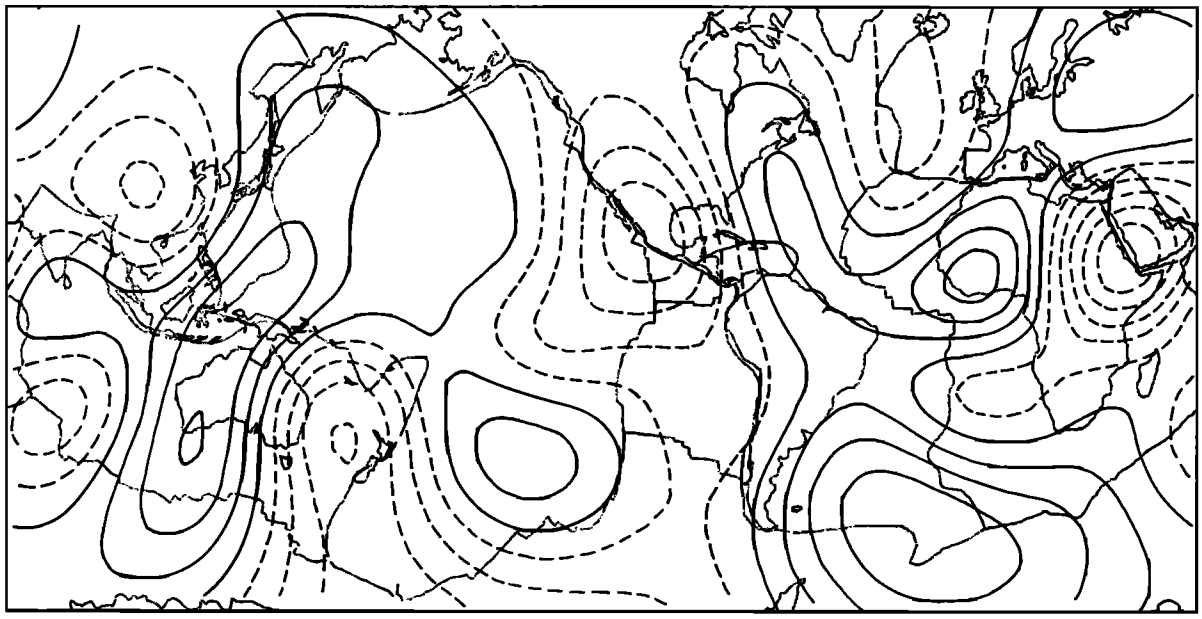

Fig. 8. Mercator projection of phase velocity variations for 200-s period Rayleigh waves for the model of *Nakanishi and Anderson* [1984]. The contour interval is 0.017 km/s; dashed lines indicate slower than average velocities, and solid lines indicate faster than average velocities.

struction of dispersed wave synthetics, it does permit a first-order appraisal of focusing and multipathing behavior caused by departure of the propagating energy from great circle paths.

We use a modified version of the surface wave ray-tracing program developed by *Sobel and von Seggern* [1978]. This program is based on the solution of the eikonal equation in spherical coordinates presented by *Julian* [1970]. The ray-

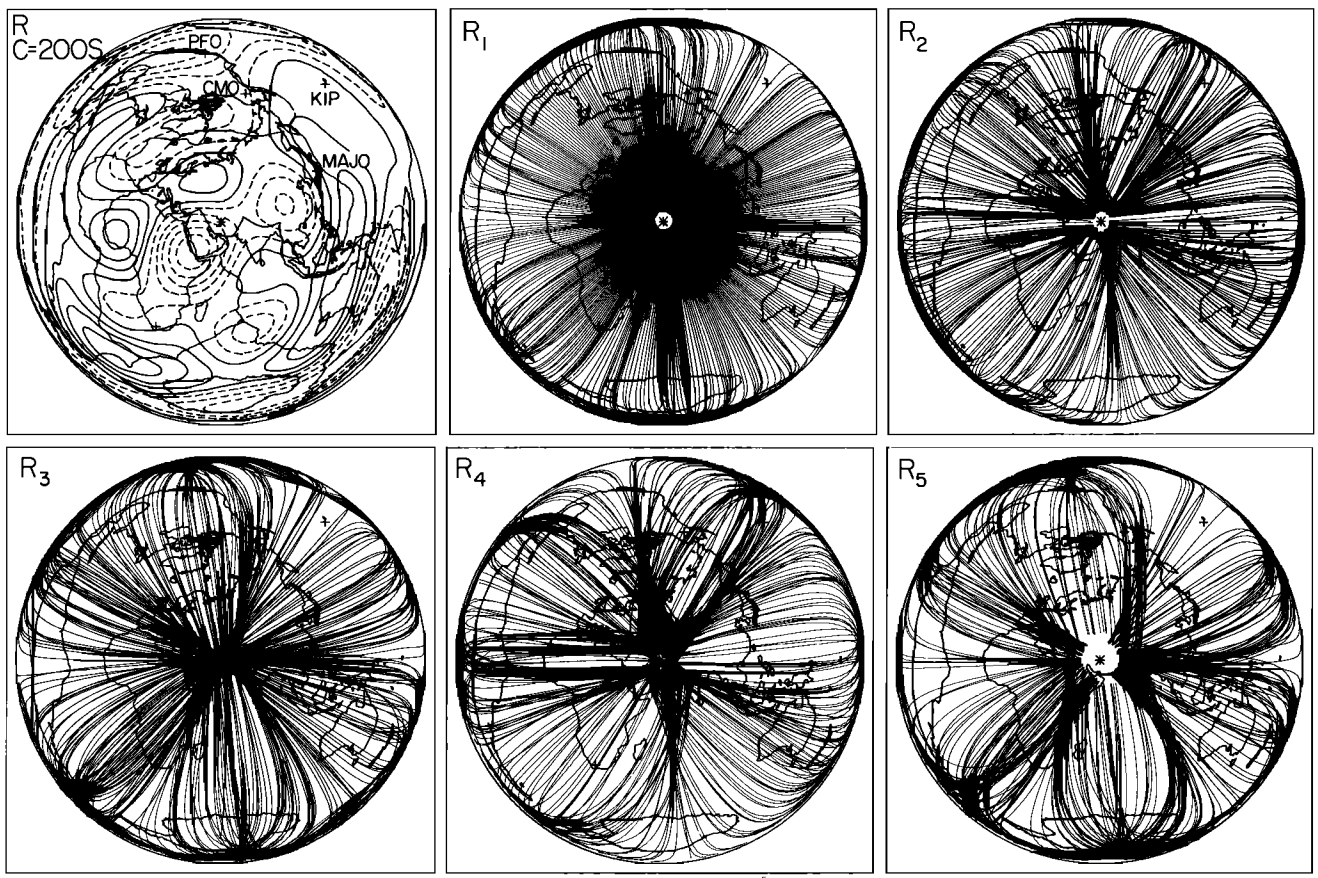

Fig. 9. Equal-area projections centered on the Iranian source region with the antipode distributed along the circumference, showing 200-s period Rayleigh wave phase velocity variations [*Nakanishi and Anderson*, 1984] and ray paths for R_1 to R_5 arrivals. Dashed contours indicate slower than average velocities, and solid contours indicate faster than average velocities. The contour interval is 0.017 km/s. The directions of the ray paths are outgoing from the center for R_1, R_3, and R_5 and incoming from the circumference for R_2 and R_4. There is a 1° increment in takeoff azimuth for the rays.

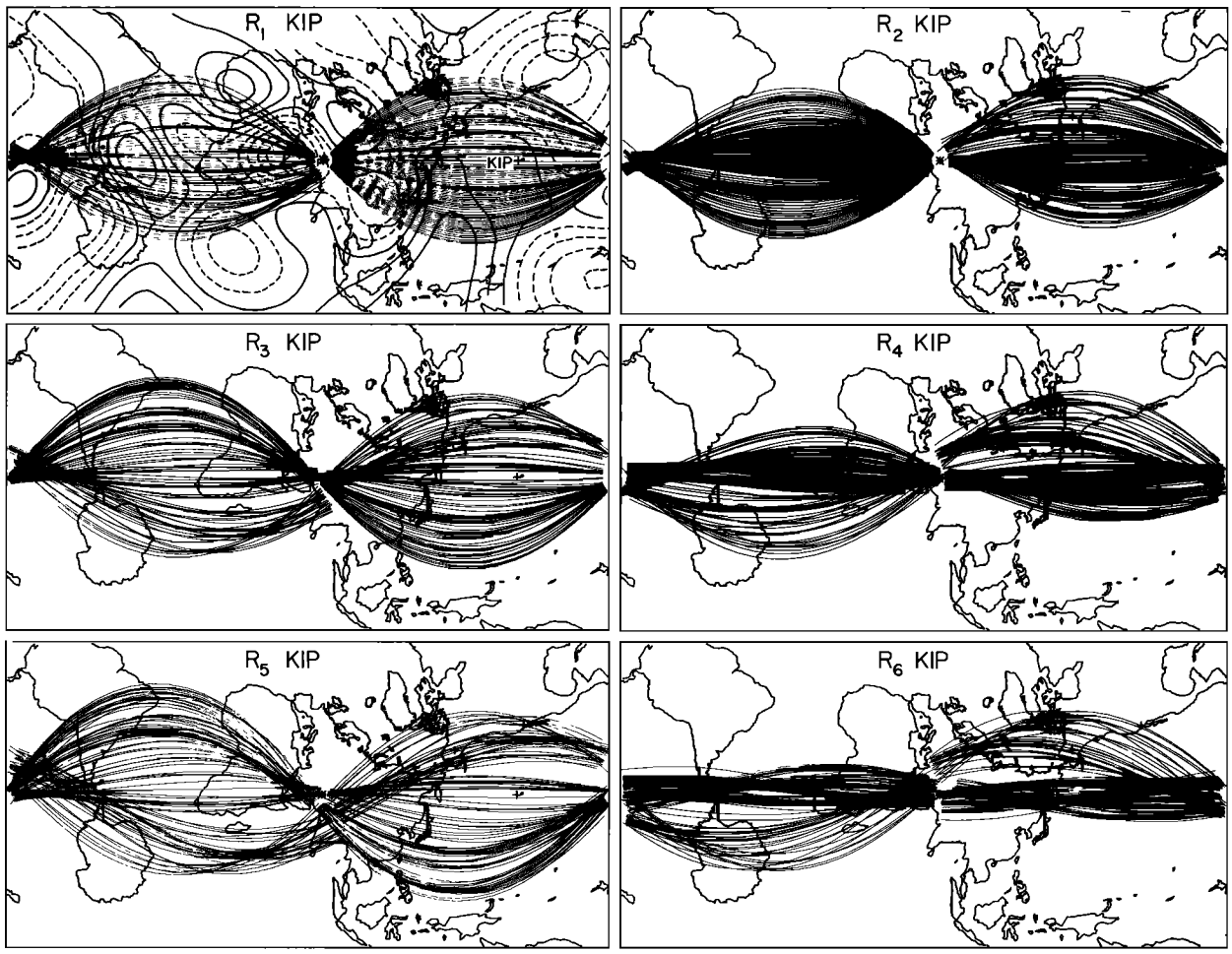

Fig. 10. Ray path plots with a 1° increment in takeoff azimuth for the 90° range in takeoff azimuth centered on the great circle between Iran and KIP. The maps are Mercator projections with the great circle from Iran to KIP as the equator. The velocity contours are the same as in Figure 9. The R_1, R_3, and R_5 rays leave the source region toward the right, along the short arc to KIP, and pass through the antipode on the left of each figure to return to the source region. The R_2, R_4, and R_6 paths leave the source region toward the left.

tracing and ray intensity equations for rays confined to travel along the surface of a sphere given by *Sobel and von Seggern* [1978] and *Julian* [1970] are appropriate for a single period. The lateral variation in phase velocity for that period must be given. The resulting phase and amplitude calculations can be directly compared with the spectra presented in the previous section. The geometric intensity calculations are invalid where caustics occur, and the calculations neglect reflected waves and mode conversions. It is also difficult to account for the lateral averaging of actual modes in the earth [*Woodhouse and Girnius*, 1982], so the amplitude comparisons must be assessed qualitatively.

Several models of global variations in phase velocity of long-period waves have been presented. Most of these are for regionalized earth models, which have sharp boundaries that are prescribed a priori [e.g., *Nakanishi and Anderson*, 1983; *Lévêque*, 1980; *Dziewonski and Steim*, 1982]. It is clearly preferable to adopt models that are free of these artificial irregularities, such as those presented by *Nakanishi and Anderson* [1984] and *Woodhouse and Dziewonski* [1984]. The latter models have smooth velocity variations but involve truncated spherical harmonic expansions of the heterogeneity. This limits their resolution of lateral variations and distributes spatially any sharp boundaries which may exist. All of these models must be viewed as preliminary at this time for there are differences between them and intrinsic limitations on their resolution. Given this situation, we adopt the spherical harmonic phase velocity expansions of *Nakanishi and Anderson* [1984] as a global model with the intent of assessing geometric effects of the heterogeneity on long-period surface wave propagation. Their model has decreasing variance reduction for periods longer than 200 s, so we will use their 200-s phase velocity structure in our calculations, and comparison will be made with observations of the same period. Since focusing effects are very sensitive to lateral gradients in velocity structure, amplitude information may potentially provide useful constraints on models of global heterogeneity, but none of the proposed models have been directly constrained by such information.

The 200-s period Rayleigh wave phase velocity variations for the model of *Nakanishi and Anderson* [1984] are contoured in Figure 8. The expansion includes harmonics up to degree $L = 6$, so the effective resolution is for structures no smaller than several thousand kilometers in extent. While this is not a complete description of the heterogeneity, there is the advantage that the long wavelengths of the velocity structure do not violate the conditions necessary for ray theory to be applied. As described by *Nakanishi and Anderson* [1984], the geographic pattern of the variations is better resolved than the amplitude of the variations. This is an important consider-

TABLE 7. Rayleigh Wave Amplitude Anomalies for Iranian Earthquakes

	Observed					Computed					
	Sept. 16, 1978			Nov. 14, 1979	Nov. 27, 1979	Intensity			Density		
	R_2	R_3	R_3/R_2	R_3/R_4	R_3/R_4	R_2	R_3	R_3/R_2	R_2	R_3	R_3/R_2
CMO	0.78	1.46	1.87	0.95*	0.82	1.69†	1.11	0.66	0.94	0.94	1.00
ESK	1.19	1.18	0.99	1.26	1.37	1.12	1.35	1.21	0.74	1.09	1.47
HAL	1.24	1.17	0.94	0.89	1.03	1.11	0.92	0.83	1.06	0.88	0.83
KIP	1.31	0.48	0.37	0.35	0.68	1.19	0.63	0.53	1.33	0.72	0.54
NNA	1.47	0.83	0.56	1.29*	1.10	0.95	0.94	0.99	0.83	0.96	1.16
PFO	1.47	1.20	0.82	0.48	0.60	1.16	1.28	1.10	1.00	1.12	1.12
RAR	1.33	0.79	0.59	1.83*	0.54	1.14	1.35	1.18	1.03	0.90	0.87
TWO	1.67	1.00	0.60	0.88*	0.60	1.02	0.74	0.73	1.00	0.65	0.65

$T = 200$ s.
*R_1/R_2 ratio is used.
†Contaminated by large amplitudes near a caustic.

ation for ray-tracing calculations, which are sensitive to velocity gradients. The velocities in Figure 8 vary over a total range of 3.4%, which is slightly larger than the typical range for regionalized models [e.g., *Nakanishi and Anderson*, 1983]. Some of the extreme values result from overshoot of the truncated harmonic expansions, but it is quite possible that the actual velocity variations are this large or even larger. To implement the ray-tracing program, we specify the phase velocities discretely for each 1° by 1° rectangular area on the earth. The general procedure we follow is very similar to that described by *Sobel and von Seggern* [1978], though we implement Runge-Kutta integrations to retain accuracy for long propagation paths.

Rayleigh wave ray paths for each 1° takeoff azimuth for 200-s period waves from the Iranian source region are shown in Figure 9. The maps are equal-area projections with the antipode distributed along the circumference. The R_1 rays are outgoing rays that travel the first 180° of distance to the antipode. The R_2 arrivals are incoming rays traveling from 180° to 360° and so on. The locations of stations with anomalous Rayleigh wave amplitude asymmetries are shown in the panel with the phase velocity variations. For a spherically symmetric velocity structure all rays would be straight radial spokes in this figure. Clearly, the heterogeneity produces progressively greater nonuniformity in the wave field for successive orbits. The phase delays accumulated are rather small on this scale, so the wavefront at any given instant is a slightly distorted concentric ring around the source region. Thus areas with a concentration of rays at a given radius would have enhanced amplitudes. Note that KIP is in a "bald" spot for odd order number arrivals but is in a ray concentration for even order number arrivals. SUR, at the southern tip of Africa, should show enhanced R_5 and R_3 amplitudes relative to R_4, as should SPA at the south pole. These predictions compare favorably with the observations in Figures 4 and 6. CMO does not have the observed asymmetry, though it lies close to areas of ray concentrations and deficiencies. By referring to Figure 3, it is possible to identify other stations at locations where asymmetries should appear if this model is correct; however, KIP stands out as the most dramatic case. We will first consider the model predictions for KIP in detail and then consider the other stations.

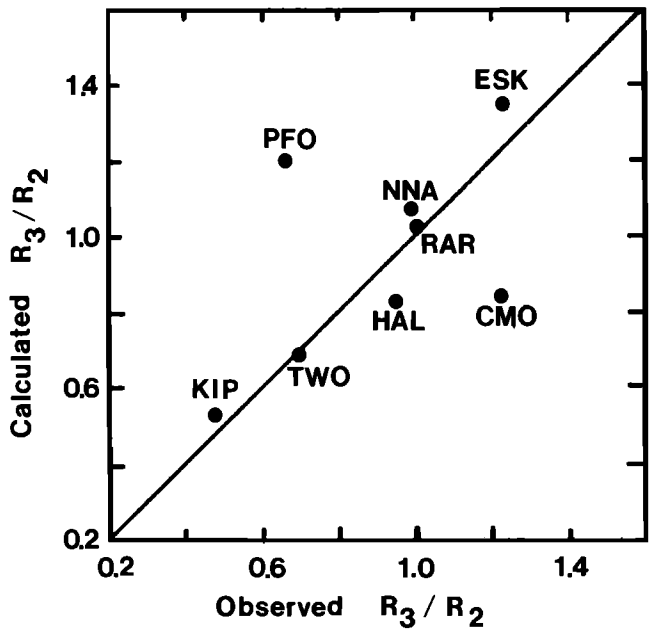

Fig. 11. Comparison of average observed and computed R_3/R_2 amplitude anomalies for the Iranian events obtained from the values in Table 7.

The pattern of asymmetry at KIP is explored further in Figure 10. The rays are projected on a Mercator projection where the equator is rotated to be the great circle connecting the Iranian source region and KIP. The left column shows the odd order number arrivals propagating along the minor arc from the source region to KIP and then continuing back around to the epicenter. The right column shows the even order number arrivals taking off to the left from the epicenter and propagating along the major arc to KIP. The rays shown span an azimuth range of 45° on either side of the great circle azimuth to KIP in 1° increments. This range in azimuth would span the loop directions in the Rayleigh wave radiation patterns for the Iranian earthquakes, as shown in Figures 4 and 6.

Several interesting phenomena are apparent in Figure 10 that would not be obvious from inspection of the velocity

TABLE 8. Calculated Rayleigh Wave Amplitude Anomalies at KIP

Method	R_1	R_2	R_3	R_4	R_5	R_6	R_3/R_2	R_5/R_4
Intensity	0.84	1.19	0.63	2.21	0.47	2.47	0.53	0.21
Density	1.00	1.33	0.72	2.06	0.50	2.56	0.54	0.24

$T = 200$ s.

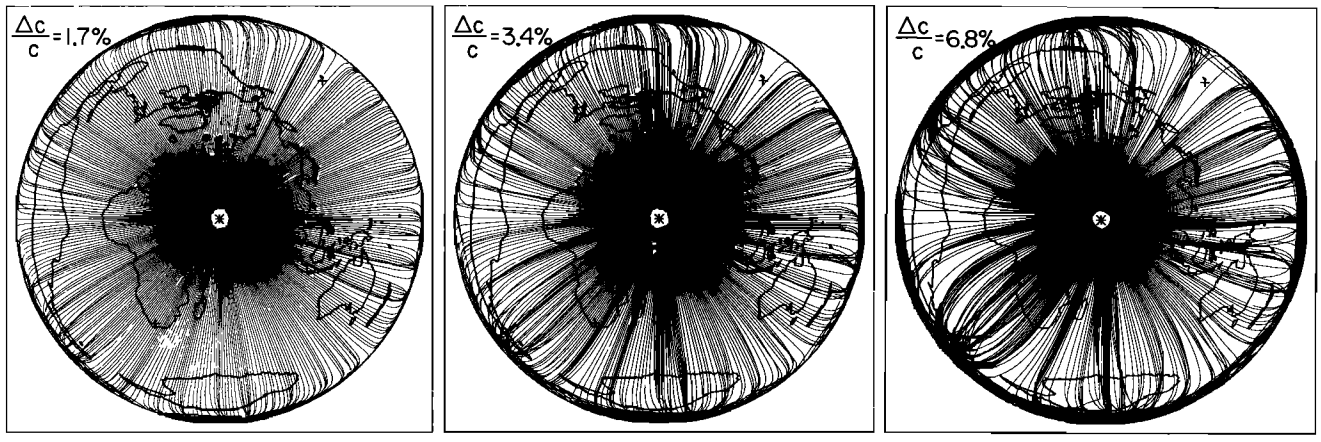

Fig. 12. R_1 ray paths traced through lateral heterogeneity models with the same geographic distribution as for the 200-s period Rayleigh wave phase velocity variations in Figure 9 but with variable peak-to-peak ranges in velocity. The range in velocity is indicated in each panel with the middle case corresponding to Figure 9.

heterogeneity. Using ray density as a guide, it is clear that even order number arrivals at KIP should be enhanced over odd order number arrivals and that there is progressive focusing and defocusing of sequential arrivals that would result in great circle Q estimates that depend upon azimuth from the source. The opposite pattern occurs at SUR at the southern tip of Africa. The ray deviations from the great circle paths can be dramatic, and there is a tendency for odd and even order number arrivals to develop complementary patterns that are relatively stable. This results from the geometry of the heterogeneity, as preferred paths are established due to the tendency for energy to move into small circles that are perpendicular to velocity gradients along most of their length. The low-velocity region in eastern Africa tends initially to focus energy leaving the source region to the southwest, while the velocity gradients across Eurasia tend to defocus energy leaving toward the northeast. This near-source geometry appears to be critical to the long-term pattern that develops and is regenerating to a certain degree for sequential orbits.

Figure 10 also shows significant spreading of the antipode and the pode for all arrivals. The ray deviations can be several thousand kilometers for R_3 arrivals. This degree of deflection is a function of the amplitude of the phase velocity variations but reflects the accumulation of small perturbations over the long propagation distances. For this case the even order number energy refocuses at the epicenter more completely than the odd order number energy. Judging from these nongeodesic features, one would expect biases in the Q measurements from antipode observations above and beyond those resulting from simple phase delays along great circle paths [*Chael and Anderson*, 1982]. The degree of bias will depend on the particular distribution of the heterogeneity as well as on the source mechanism, which determines the amplitude weighting of each ray.

While the velocity structure of *Nakanishi and Anderson* [1984] provides qualitative agreement with the observed amplitude asymmetry at KIP, it is of interest to compare the results for other stations. It is reasonable to expect that most amplitude anomalies will not be predicted because the velocity structures are still preliminary and are heavily smoothed. Table 7 and Figure 11 compare amplitude anomalies observed for the Iranian earthquakes with the ray-tracing predictions calculated by two methods. The observed anomalies are defined, as they were in Table 3, by the ratio of the observed 200-s period amplitudes to those calculated for a fault inversion of the Rayleigh and Love waves spectra of that period. The two methods used to calculate the ray-tracing amplitudes involve ray intensity and ray density. In the former procedure the contributions of ray intensities, weighted linearly by distance from the receiver, for all rays within one wavelength from the station at the time that the wave front passes it are summed. This sum is normalized by the corresponding sum for a homogeneous earth, and the square root is taken. The ray density anomalies are simply the ratios of the number of rays within one wavelength of the station as the wave front passes for the heterogeneous and homogeneous models. In both procedures we are attempting to account for the lateral averaging properties of the surface waves as well as the focusing and multipathing effects. The intensity calculations are unstable near caustics, but the ray density calculation is well behaved for such cases. Other procedures such as Gaussian beam computation [*Jobert and Jobert*, 1983; *Yomogida*, 1983] or more rigorous wave theory [*Park et al.*, 1983; *Tanimoto*, 1983] could provide more accurate amplitude estimates for our models, but we are only interested in first-order features, which are well characterized by ray density. An interesting aspect of the ray calculations is that sequential arrivals such as R_2 and R_4 do not necessarily involve the same set of rays for the rays that actually intersect the station may leave the source at slightly different azimuths.

The comparisons in Table 7 and Figure 11 are not very close in detail, and there is little reason to expect them to be particularly good. However, the range in variations is similar, indicating that the 3.4% phase velocity heterogeneity in the *Nakanishi and Anderson* [1984] structure can account for the amplitude variations. The computed anomalies have the correct sign and amplitude for HAL, ESK, KIP, and TWO, but the anomaly at PFO is not matched. Note that the observations fluctuate for CMO, NNA, and RAR (Table 7), which may be due to the differences in source location. The complexity of the raypaths in Figure 9 can be very sensitive to source location because some caustics are quite close to regions with diminished amplitudes and small differences in location can shift the patterns significantly. The ray intensity and ray density calculations give comparable amplitude estimates except when a caustic develops close to the receiver, as is the case for R_2 at CMO. In these amplitude calculations no attempt was made to introduce radiation pattern weighting to the ray amplitudes. This is probably not very significant for stations in loop directions of the radiation pattern but may be

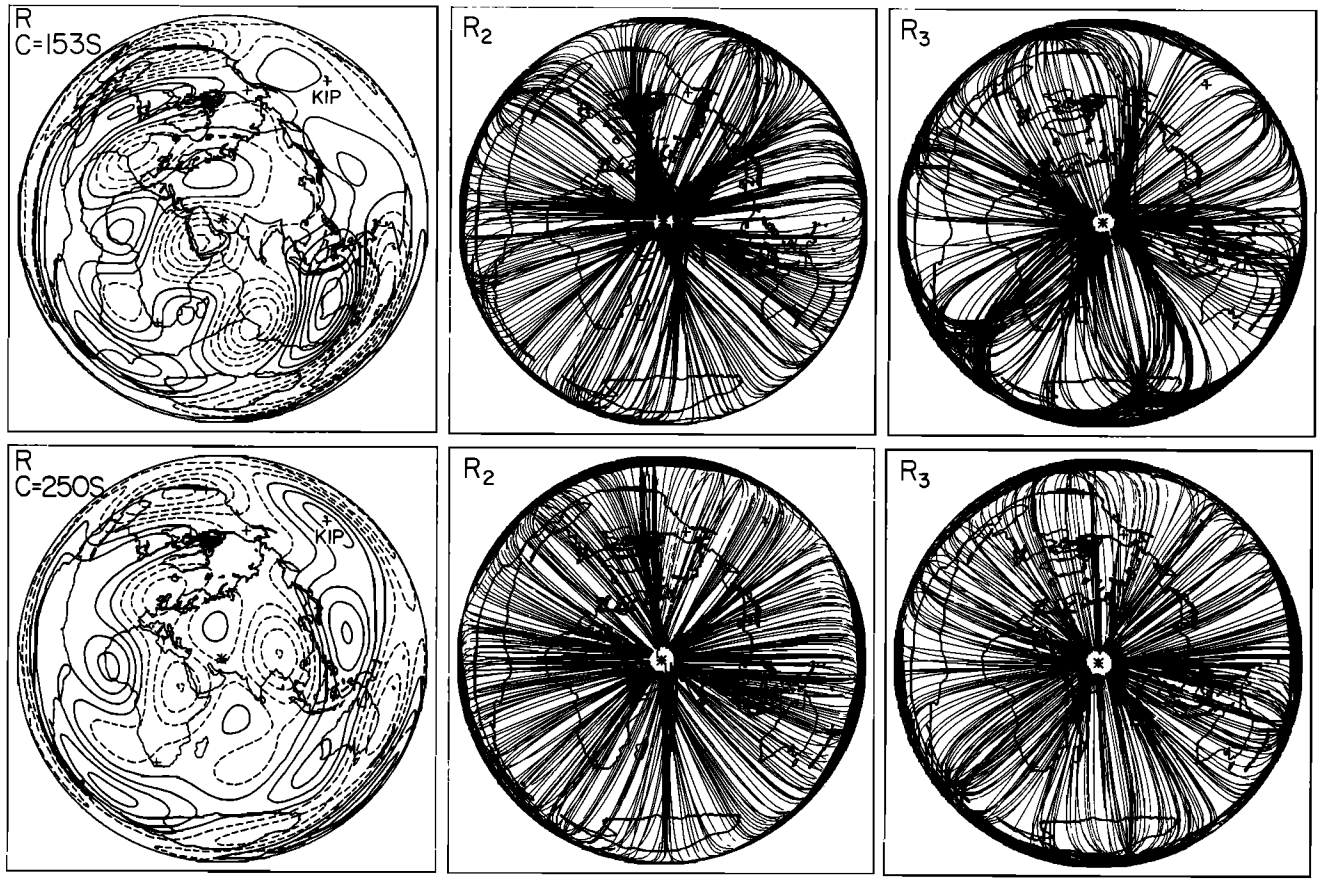

Fig. 13. Rayleigh wave phase velocity variations and R_2 and R_3 ray paths with the same conventions as in Figure 9 but for periods of 153 and 250 s.

important for stations near nodes of the radiation pattern that receive rays deflected from loop directions. This effect should be most apparent for stations near the epicenter or the antipode.

The ray-tracing amplitude predictions for the first six Rayleigh wave arrivals at KIP are shown in Table 8. The increasing anomaly for both odd and even order arrivals produces somewhat stronger asymmetries for R_5/R_4 than observed (Table 3). To appraise the effect of reducing the phase velocity heterogeneity, we trace rays through structures with the same geographic variations but varying peak-to-peak ranges in velocity. Figure 12 shows R_1 arrivals for three cases. The middle case, and the geographic variation for all three cases, is the same as for the 200-s period phase velocities in Figure 9. Halving the range of velocity variation clearly reduces the ray deflections substantially, while doubling the range increases the ray deviations correspondingly. In all three cases, KIP locates in a low-amplitude region for R_1 and successive odd order number arrivals. The R_1 amplitude anomaly increases from 0.90 to 0.84 to 0.72 as the range in velocity increases from 1.7 to 3.4 to 6.8%, respectively. This defines a linear relation with negative slope between amplitude and $\Delta C/C$, which in turn reflects the relation between amplitude and the second spatial derivative of the velocity gradient transverse to the direction of propagation [e.g., *Wong and Woodhouse*, 1983].

It is also important to address the stability of the ray-tracing amplitude anomalies for different periods. The phase velocity models of *Nakanishi and Anderson* [1984] show some variations in geographic distribution from period to period. Presumably, this reflects the different depth sampling for each period but also may include the variation in measurement accuracy and source effects for each frequency. The global phase velocity distributions and corresponding R_2 and R_3 ray paths are shown for 153- and 250-s period Rayleigh waves in Figure 13. Note that the range in phase velocity is greater for shorter periods, being 4.4 and 2.9% for 153-s and 250-s periods respectively. The regional variations have some differences from those for a 200-s period (Figure 9) for both cases but differ most at the longer period. The predicted R_3/R_2 amplitude anomaly at KIP is 0.58 for a 153-s period, which is

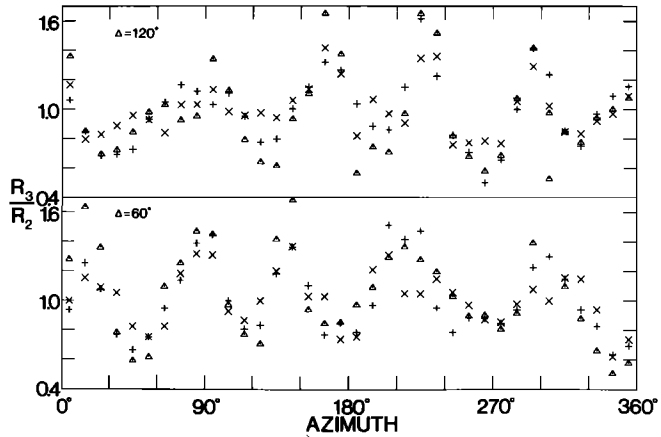

Fig. 14. Azimuthal variation of predicted R_3/R_2 amplitude ratios for periods of 153 (triangles), 200 (pluses), and 250 s (crosses) at distances from the Iranian source region of 60° (bottom) and 120° (top).

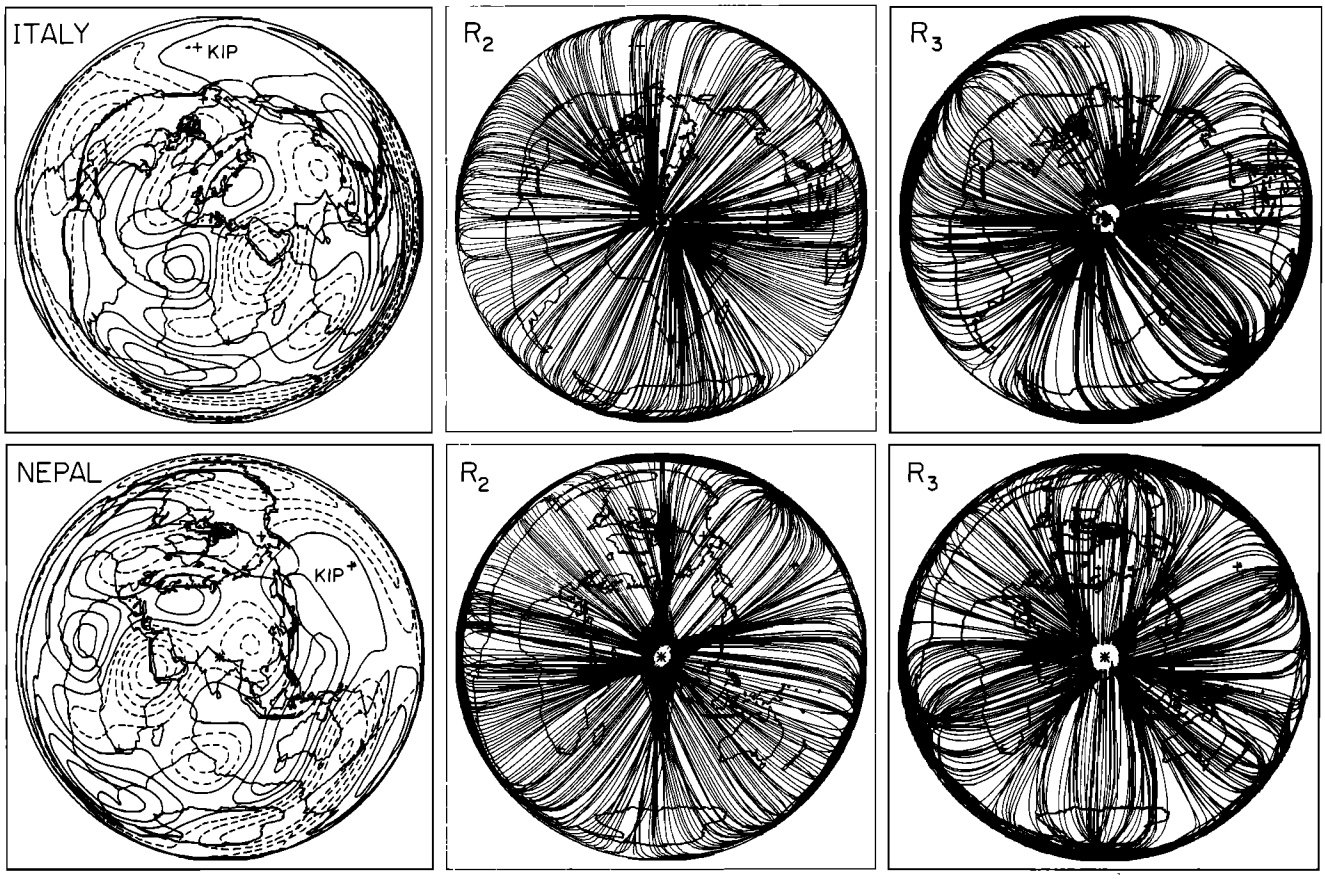

Fig. 15. Rayleigh wave phase velocity variations and R_2 and R_3 ray paths for a period of 200 s with the same conventions as in Figure 9 but for the Italy and Nepal source region.

close to the value of 0.54 for a 200-s period. On the other hand, the 250-s period rays give an R_3/R_2 ratio of 1.39, opposite in sense to both the shorter-period calculations and the observations. Figure 14 shows the azimuthal variation of predicted R_3/R_2 amplitude ratios at distances of 60° and 120° from the Iranian source region. As expected, the 153-s period waves have somewhat greater amplitude variations, while the long-wavelength azimuthal patterns are similar for each period. The distance dependence of the R_3/R_2 amplitude ratios is clearly evident. The decrease in variance reduction in the global inversions of *Nakanishi and Anderson* [1984] for periods longer than 200-s may indicate that the longer-period structure is more poorly resolved. However, Figure 13 does illustrate the sensitivity of the ray path complexity to fairly subtle variations in the heterogeneity. These results may be taken as evidence that the successful prediction of the observed KIP asymmetry at shorter periods is fortuitous. Even if this is the case, these calculations provide examples of the qualitative effects of realistic global heterogeneity on long-period surface wave propagation.

Rayleigh wave ray paths for 200-s period energy for the Italian and Nepal source regions are shown in Figure 15. Comparison of these plots with Figure 9 illustrates how sensitive the ray complexity is to the configuration of the heterogeneity with respect to the source region. An important point to note is that none of the stations in Figure 3 lie in a location where asymmetry as strong as that for KIP for the Iranian source region is expected. In fact, for the Italian source region as well as for other Mediterranean sources the calculated R_3/R_2 asymmetry at SUR, PFO, CMO, and KIP is always less than 20%. For the Nepal event the predicted amplitude ratio of R_3/R_2 for KIP is 1.46, which is opposite in sense to the Iranian anomalies. Unfortunately, the KIP recording was not usable for this event. The computed amplitude ratios at other stations for the Nepal event vary more than for the Mediterranean sources, but there is little correspondence with the observed variations. The asymmetries at SUR and ANMO apparent in Figure 7*c* are opposite in sense to the predicted values of $R_2/R_1 = 1.16$ for ANMO and $R_3/R_2 = 1.17$ for SUR, though the CMO prediction is consistent ($R_3/R_2 = 1.18$). In general, the predicted amplitude asymmetries for these two source regions are significantly smaller than for the KIP path for the Iranian source region. This argues against the latter prediction being a purely fortuitous result.

In all of the source mechanism inversions described in the previous section, the scatter in Love wave phase and amplitudes was significantly greater than for Rayleigh waves with the same period. Figure 16 illustrates how this could be the result of global heterogeneity. The figure shows ray paths for the 200-s period Love wave phase velocity structure of *Nakanishi and Anderson* [1984]. The range in phase velocity is 4.5% compared with 3.4% for 200-s period Rayleigh waves. The deviations from great circle paths are correspondingly larger, but once again, KIP lies in a region of strong asymmetry with $G_3/G_2 = 0.58$. This results from the similarity of the geographic variations in phase velocity across Africa and Eurasia for the Rayleigh and Love waves. The G_3/G_2 ratio predicted for ANMO is 0.47, which compares favorably with the observations in Figures 4 and 6. Smaller asymmetries are predicted for other stations, but the overall tendency is for asymmetries to be larger and more pervasive than for the Rayleigh waves.

Judging from the ray plots in Figures 9–16, there is good

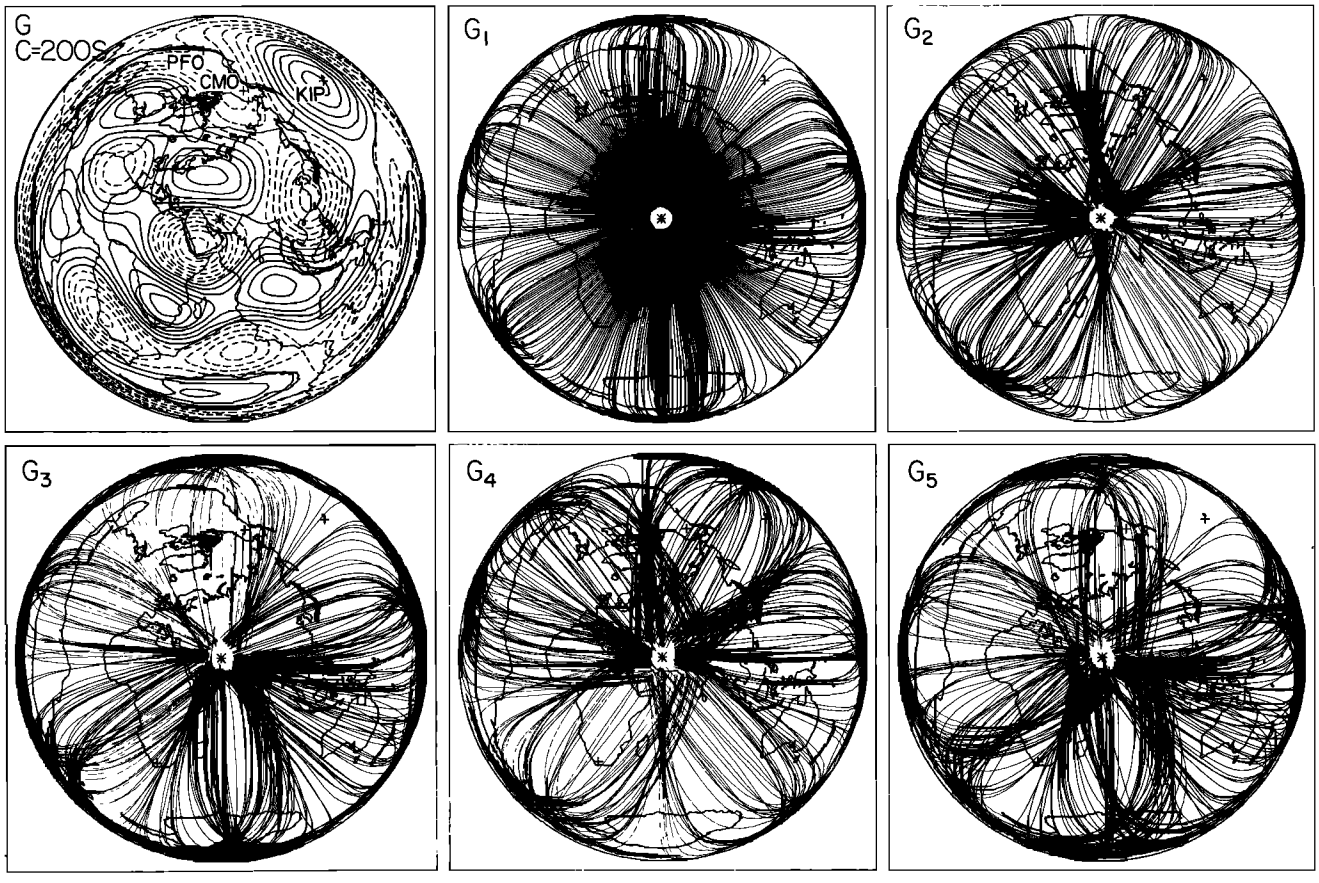

Fig. 16. Love wave phase velocity variations and G_1 to G_5 ray paths for a period of 200 s for the Iranian source region with the same conventions as in Figure 9.

reason to expect amplitude asymmetries to be observed for many earthquakes. This is in fact the case [e.g., *Park et al.*, 1983; *Tanimoto*, 1983]; however, few examples as dramatic as for the Iranian events have been published. Here we discuss several anomalous observations that we have encountered in routine moment tensor inversions of large earthquakes. Figure 17 shows Rayleigh wave observations for the Akita-Oki, Japan, earthquake that occurred on May 26, 1983. Stations GUA and CTAO, lying at azimuths near N170°E, show anomalously small R_3/R_2 and R_5/R_4 amplitude ratios. To calibrate the GUA observation, we include the recording at station KMY, which has almost the same epicentral separation as GUA. KMY shows normal relative amplitude behavior between the minor arc and major arc arrivals, with perhaps a slight enhancement of the odd order number arrivals. Stations TWO and SNZO bracket GUA and CTAO tightly in azimuth but show less asymmetry. ESK lies opposite in azimuth to these stations and shows normal amplitude behavior, complicating any attempt to explain the asymmetry by source finiteness.

Ray paths for the 200-s period phase velocity structure of *Nakanishi and Anderson* [1984] for R_2 and R_3 arrivals from the Japan source region are shown in Figure 18. Stations CTAO and GUA lie near a caustic for R_2 arrivals and are deficient in ray density for R_3 arrivals. This asymmetry is less pronounced for SNZO and TWO, while ESK has similar ray density for R_2 and R_3. A slight enhancement of R_3 over R_2 amplitudes is also expected for KMY. Thus, qualitatively, the ray-tracing predictions agree with the observations. Comparing Figures 9, 13, and 18, it appears that the global heterogeneity has greater influence on signals from the Japanese source region. This stems from the large number of great circle paths with strong transverse velocity gradients, as shown in Figure 18. While the Japan source region lies close to the great circle between Iran and KIP (Figure 10), the ray calculations predict that R_3 should be slightly enhanced relative to R_2 at KIP, as is actually observed. In fact, R_5 is much larger than R_4 in the data from KIP. This is opposite to the Iranian event asymmetry, which illustrates the importance of the near source region heterogeneity as well as the focusing characteristics for velocity anomalies in the spherical earth.

The February 28, 1979, St. Elias, Alaska, earthquake also produced some anomalous records. The PFO recording for this event, with successive broadband and narrow-band Gaussian filters is shown in Figure 19. There is a persistent asymmetry between odd and even order number arrivals for periods up to 250 s. While source directivity could produce this asymmetry, the aftershocks indicate a fault length of only 50–115 km [*Stephans et al.*, 1980]. Unless this length is grossly underestimated, very slow rupture velocities would have to be appealed to in order to explain the asymmetry (S. Grand, personal communication, 1983). As for the Japan source region, the Alaskan source region has strong velocity gradients transverse to many of the great circle paths (Figure 20). The 200-s period phase velocity variations around the source region and ray paths for R_4 and R_5 are shown in Figure 20. Strong amplitude asymmetries are expected for circum-Pacific stations, though PFO is not predicted to have the observed relative enhancement of R_5. This may well reflect the inadequacy of the velocity model, which does not have velocity

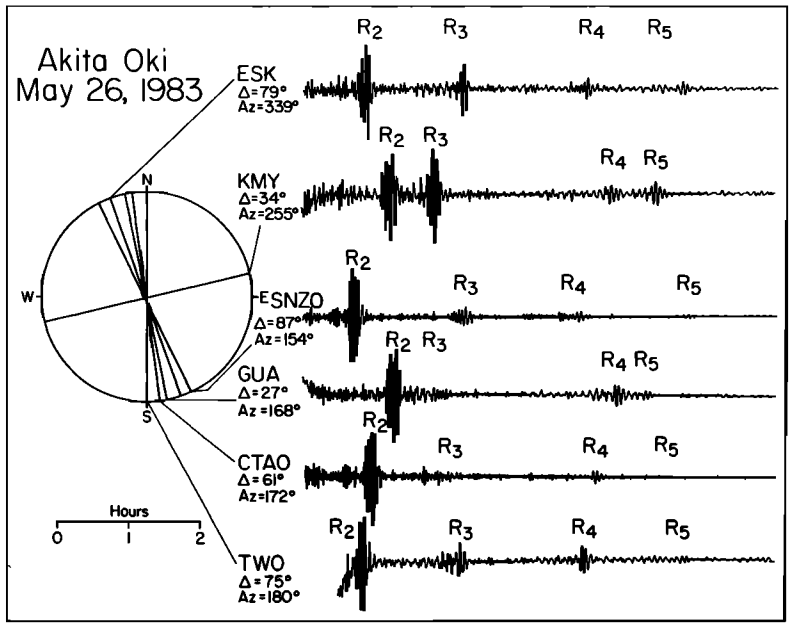

Fig. 17. Rayleigh wave recordings of the Akita-Oki earthquake showing the anomalous R_3/R_2 observations for stations near an azimuth of N170°E.

gradients across North America consistent with the known strong variations in shear velocity across the Rocky Mountain front. If the velocity heterogeneity were rotated just a few degrees clockwise, PFO would have $R_5 > R_4$ predicted. Improved resolution of the velocity models will be required for analysis of such long propagation paths.

Discussion

The successful predictions of the amplitude asymmetries at KIP for Iranian earthquakes and for the Akita-Oki observations discussed above are clearly dependent upon the accuracy of the phase velocity models of *Nakanishi and Anderson* [1984]. An independent test of these models can be obtained by comparing their phase velocity variations with those found by *Woodhouse and Dziewonski* [1984]. For periods around 200 s the models are quite compatible in terms of long-wavelength features. Figure 9 of *Woodhouse and Dziewonski* [1984] shows phase velocity variations for ${}_0S_{40}$ (period = 212 s), which can be compared with Figures 9, 10, and 16 in this paper or corresponding Figures 9 and 20 of *Nakanishi and Anderson* [1984]. The large, low-velocity region in eastern Africa and Saudi Arabia and the velocity gradients across Eurasia and the Indian Ocean are very similar for both models. Since these features are important for establishing the KIP asymmetry, it seems likely that similar asymmetries will be predicted by both models. Preliminary calculations indicate that the sign of the asymmetries, but not their amplitudes, for the KIP, CMO, and PFO observations for the 1978 Tabas event are predicted by the model of *Woodhouse and Dziewonski* [1984] (J. Woodhouse, personal communication, 1983). This will be tested further in the future, though clearly both models are only preliminary attempts to define the global variations. The phase velocity variations found by *Woodhouse and Dziewonski* [1984] do have somewhat smaller ranges ($\simeq$ 3.0% for ${}_0S_{40}$ and 4.5% for ${}_0T_{40}$) compared with those in the *Nakanishi and Anderson* [1984] model, but these are still large enough to cause significant great circle deviations.

A question that naturally arises is whether or not the substantial ray path deviations predicted by the laterally heterogeneous structures are sufficient to violate the great circle assumption made in the derivation of the structures. When we calculate great circle phase velocities from sequential odd or

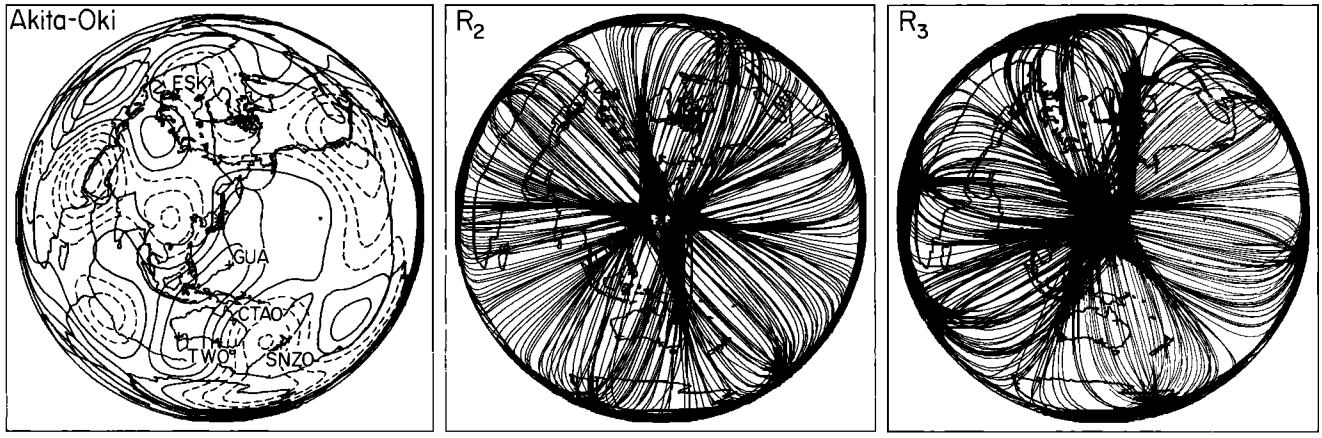

Fig. 18. Rayleigh wave phase velocity variations and R_2 and R_3 ray paths for a period of 200 s for the Akita-Oki source region with the same conventions as in Figure 9.

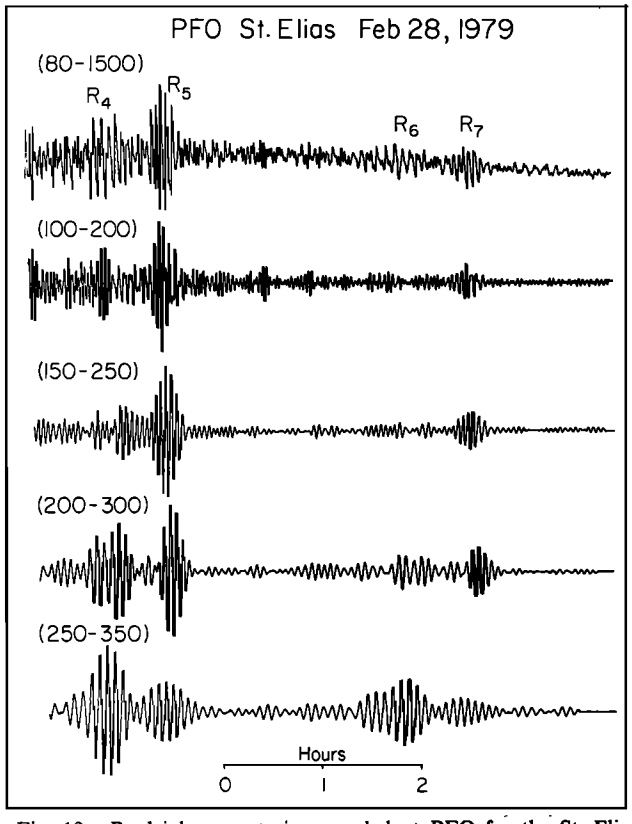

Fig. 19. Rayleigh wave train recorded at PFO for the St. Elias earthquake with different Gaussian band-pass filter. The asymmetry between minor and major arc arrivals persists to a period of 250 s.

even number arrivals for the ray-tracing models, we find stable estimates despite the fact that different rays actually reach the receiver for each arrival. The phase delays for individual arrivals tend to be small as well, even when there is significant contortion of the wave front. It seems that the greatest source of bias may be due to the tendency for odd and even order number arrivals to settle into complementary small circle orbits. While the phase anomalies are self-regulating to a large degree, the inversion techniques which distribute the anomaly along the great circle regardless of order number may be placing the anomaly in the wrong location or canceling out the actual variations. An attempt to include the actual ray paths in inversion for lateral heterogeneity will be made in a future paper to quantify these effects. While the effects on existing long-period (>200 s) models should be minor, the increased phase velocity variations for shorter periods may cause significant revisions. Future efforts to invert for higher-order spherical harmonic expansions or grid models of the heterogeneity will have to account for non-great circle effects for medium-period (50–200 s) surface waves.

Eventually, it may be possible to incorporate surface wave amplitude information into inversions for lateral heterogeneity or at least to test models for their ability to reduce the scatter in the observations. An important consideration is the effect of the amplitude variations on Q estimates for spheroidal and toroidal modes. Given the relatively high Q values of these modes, small (20%) amplitude asymmetries due to propagation can result in erroneous Q estimates. For a great circle of length l, with a great circle group velocity U, the great circle Q is determined from

$$Q = -\frac{\pi l}{UT \ln \xi}$$

T is the period and ξ is the amplitude ratio

$$\xi = \frac{a_{i+2}}{a_i}$$

where a_i is the spectral amplitude of the ith order surface wave. For a uniform earth, with no velocity heterogeneity effects on the amplitudes, we have the "intrinsic" attenuation given by

$$Q_0 = -\frac{\pi l}{U_0 T \ln \xi_0}$$

Defining the ratios of the actual amplitudes in the laterally varying earth to those for the uniform earth by

$$E_i = a_i/a_{i,0}$$

$$E_{i+2} = a_{i+2}/a_{i+2,0}$$

we obtain

$$\xi = \frac{E_{i+2}}{E_i}\,\xi_0$$

Neglecting differences between U and U_0, we have

$$\frac{Q}{Q_0} \simeq \frac{\ln \xi_0}{\ln \xi} \simeq \left[1 + \left(\ln \frac{E_{i+2}}{E_i} \ln \xi_0\right)\right]^{-1}$$

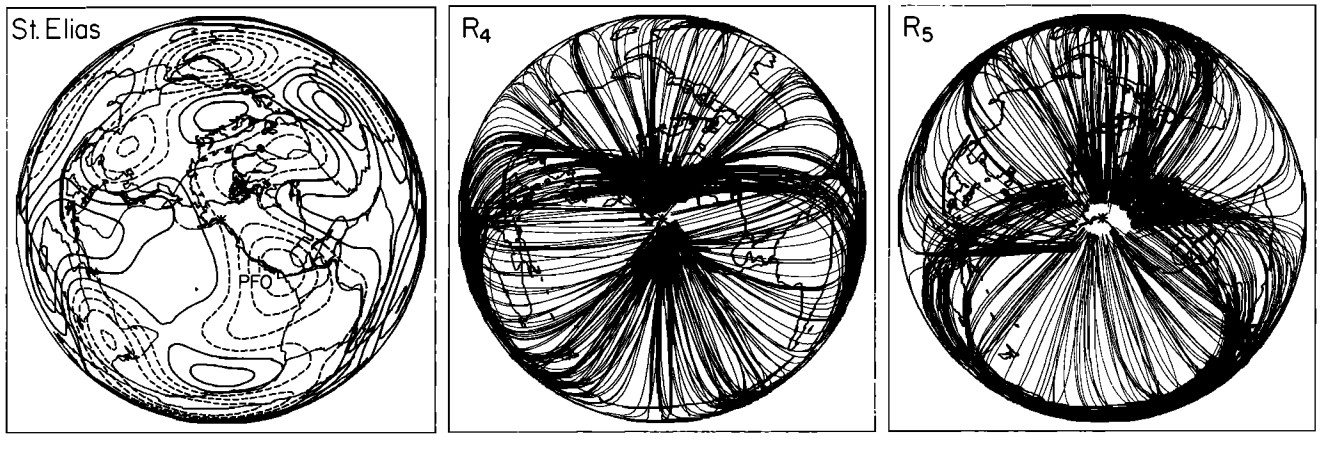

Fig. 20. Rayleigh wave phase velocity variations and R_4 and R_5 ray paths for a period of 200 s for the St. Elias source region with the same conventions as in Figure 9.

For spheroidal and toroidal modes with periods of 200.9 s we have $\zeta_0 = 0.32$ and 0.28 and $Q_0 = 154$ and 111, respectively. We use the computed ray density anomalies (E_i) in Table 8 to test the bias in Q determination. From R_3/R_1 or R_5/R_3 we obtain $Q/Q_0 = 0.8$, while from R_4/R_2 we get $Q/Q_0 = 1.6$. Thus, for this case the asymmetric and progressive effects of the heterogeneity give a range in Q of from 123 to 246 for the same great circle. The variation in Q estimates for a fixed great circle and between closely adjacent great circles seen in Table 6 indicates that such effects are common. The problems with determining short-arc Q values are correspondingly greater.

CONCLUSIONS

Surface wave ray-tracing calculations for models of global phase velocity variations proposed by *Nakanishi and Anderson* [1984] show that large-amplitude anomalies will be observed for Love and Rayleigh waves with periods of 100–250 s. These anomalies are most directly manifested in asymmetry of minor arc and major arc arrivals at a given station. The spatial distribution of velocity heterogeneity about a given source region governs the development of such anomalies. Source regions for which great circle paths encounter large transverse velocity gradients will have more pronounced anomalies. The amplitude variations produced by focusing and multipathing cause scatter in Q determinations. The deviation from great circle behavior may be large enough to affect inversions for lateral velocity variations, particularly for shorter periods. Several of the more pronounced amplitude anomalies observed for events in Iran and Japan are well predicted by the ray calculations for the *Nakanishi and Anderson* [1984] models for periods of 200 s. However, some anomalies are not predicted, and improved velocity models will have to be developed before the scatter in long-period amplitudes can be reliably reduced.

Acknowledgments. We thank Ichiro Nakanishi for providing us with his spherical harmonic expansions and the code for constructing the velocity variations. Dave von Seggern kindly provided us with his ray-tracing code. Don Anderson made useful suggestions about the presentation of the ray paths. John Woodhouse provided preliminary amplitude calculations for the Harvard model of aspherical heterogeneity. Rob Van der Voo and three anonymous reviewers provided constructive reviews. This research was supported by the Division of Earth Sciences, National Science Foundation grants EAR-8116023 and EAR-8317623, U.S. Geological Survey grant 14-08-0001-G-814, and NASA contract NSG-7610. Contribution 4052, Division of Geological and Planetary Sciences, California Institute of Technology, Pasadena, California.

REFERENCES

Berberian, M., I. Asudeh, R. G. Bilham, C. H. Scholtz, and C. Soufleris, Mechanism of the main shock and the aftershock study of the Tabas-e Golshan (Iran) earthquake of September 16, 1978: A preliminary report, *Bull. Seismol. Soc. Am.*, *69*, 1851–1859, 1979.

Buland, R., and J. Taggart, A mantle wave magnitude for the St. Elias, Alaska, earthquake of 28 February, 1979, *Bull. Seismol. Soc. Am.*, *71*, 1143–1159, 1981.

Capon, J., Analysis of Rayleigh wave multipath propagation at LASA, *Bull. Seismol. Soc. Am.*, *60*, 1701–1731, 1970.

Chael, E. P., and D. L. Anderson, Global Q estimates from antipodal Rayleigh waves, *J. Geophys. Res.*, *87*, 2840–2850, 1982.

Dziewonski, A. M., and J. M. Steim, Dispersion and attenuation of mantle waves through waveform inversion, *Geophys. J.R. Astron. Soc.*, *70*, 503–527, 1982.

Dziewonski, A. M., and J. H. Woodhouse, An experiment in systematic study of global seismicity: Centroid-moment tensor solutions for 201 moderate and large eqrthquakes of 1981, *J. Geophys. Res.*, *88*, 3247–3271, 1983.

Dziewonski, A. M., A. Friedman, D. Giardini, and J. H. Woodhouse, Global seismicity of 1982: Centroid-moment tensor solutions for 308 earthquakes, *Phys. Earth Planet. Inter.*, *33*, 76–90, 1983.

Gjevik, B., Ray tracing for seismic surface waves, *Geophys. J. R. Astron. Soc.*, *39*, 29–39, 1974.

Haghipour, A., and M. Amidi, The November 14 to December 25, 1979 Ghaenat earthquakes of northeast Iran and their tectonic implications, *Bull. Seismol. Soc. Am.*, *70*, 1751–1757, 1980.

Jobert, N., and G. Jobert, An application of ray theory to the propagation of waves along a laterally heterogeneous spherical surface, *Geophys. Res. Lett.*, *10*, 1148–1151, 1983.

Julian, B. R., Ray tracing in arbitrarily heterogeneous media, *Tech. Note 1970-45*, Lincoln Lab., Lexington, Mass., 1970.

Kanamori, H., Velocity and Q of mantle waves, *Phys. Earth Planet. Inter.*, *2*, 259–275, 1970.

Kanamori, H., and J. W. Given, Use of long-period surface waves for rapid determination of earthquake source parameters, *Phys. Earth Planet. Inter.*, *27*, 8–31, 1981.

Kanamori, H., and J. W. Given, Use of long-period surface waves for rapid determination of earthquake source parameters, 2, Preliminary determination of source mechanisms of large earthquakes ($M_s \geq 6.5$) in 1980, *Phys. Earth Planet. Inter.*, *30*, 260–268, 1982.

Lay, T., J. W. Given, and H. Kanamori, Long-period mechanism of the 8 November 1980 Eureka, California earthquake, *Bull. Seismol. Soc. Am.*, *72*, 439–456, 1982.

Lévêque, J. J., Regional upper mantle S-velocity models from phase velocities of great-circle Rayleigh waves, *Geophys. J. R. Astron. Soc.*, *63*, 23–43, 1980.

Masters, G., T. H. Jordan, P. G. Silver, and F. Gilbert, Aspherical earth structure from fundamental spheroidal-mode data, *Nature*, *298*, 609–613, 1982.

McGarr, A., Amplitude variations of Rayleigh waves—Horizontal refractions, *Bull. Seismol. Soc. Am.*, *59*, 1307–1334, 1969.

Nakanishi, I., and D. L. Anderson, World-wide distribution of group velocity of mantle Rayleigh waves as determined by spherical harmonic inversion, *Bull. Seismol. Soc. Am.*, *72*, 1185–1194, 1982.

Nakanishi, I., and D. L. Anderson, Measurements of mantle wave velocities and inversion for lateral heterogeneity and anisotropy, 1, Analysis of great circle phase velocities, *J. Geophys. Res.*, *88*, 10267–10283, 1983.

Nakanishi, I., and D. L. Anderson, Measurements of mantle wave velocities and inversion for lateral heterogeneity and anisotropy, II, Analysis by the single-station method, *Geophys. J. R. Astron. Soc.*, *78*, 573–617, 1984.

Niazi, M., and H. Kanamori, Source parameters of 1978 Tabas and 1979 Qainat, Iran, earthquakes from long-period surface waves, *Bull. Seismol. Soc. Am.*, *71*, 1201–1213, 1981.

Park, J., G. Masters, and F. Gilbert, The effects of source mechanism on surface waves for an aspherical earth model, *Eos Trans. AGU*, *64*, 754, 1983.

Silver, P. G., and T. H. Jordan, Fundamental spheroidal mode observations of aspherical heterogeneity, *Geophys. J. R. Astron. Soc.*, *64*, 605–634, 1981.

Sobel, P. A., and D. H. von Seggern, Application of surface wave ray tracing, *Bull. Seismol. Soc. Am.*, *68*, 1359–1380, 1978.

Stephans, C. D., J. C. Lahr, K. A. Fogleman, and R. B. Horner, The St. Elias, Alaska, earthquake of February 28, 1979: Regional recording of aftershocks and short-term, pre-earthquake seismicity, *Bull. Seismol. Soc. Am.*, *70*, 1607–1633, 1980.

Tanimoto, T., Inversion of mantle Love waves for lateral heterogeneity and spherically symmetric Q: The Born seismogram approach, *Eos Trans. AGU*, *64*, 755, 1983.

Wong, Y. K., and J. H. Woodhouse, Ray theory for surface waves on a sphere, *Eos Trans. AGU*, *64*, 260, 1983.

Woodhouse, J. H., The joint inversion of seismic waveforms for lateral variations in earth structure and earthquake source parameters, *Proc. Int. Sch. Phys. Enrico Fermi*, *85*, 366–397, 1983.

Woodhouse, J. H., and A. M. Dziewonski, Mapping the upper mantle: Three-dimensional modeling of earth structure by inversion of seismic waveforms, *J. Geophys. Res.*, *89*, 5953–5986, 1984.

Woodhouse, J. H., and T. P. Girnius, Surface waves and free oscillations in a regionalized earth model, *Geophys. J. R. Astron. Soc.*, *68*, 653–674, 1982.

Yomogida, K., The detection of surface wave velocity anomalies: Ray-theoretical approach, *Eos Trans. AGU*, *64*, 755, 1983.

H. Kanamori, Seismological Laboratory, California Institute of Technology, Pasadena, CA 91125.

T. Lay, Department of Geological Sciences, University of Michigan, 1006 C. C. Little Building, Ann Arbor, MI 48109.

(Received March 9, 1984;
revised July 23, 1984;
accepted August 17, 1984.)